ORCA – Online Research @ Cardiff

This is an Open Access document downloaded from ORCA, Cardiff University's institutional repository:https://orca.cardiff.ac.uk/id/eprint/85102/

This is the author's version of a work that was submitted to / accepted for publication.

Citation for final published version:

Schepelmann, M. , Yarova, P. L., Lopez-Fernandez, I., Davies, T. S., Brennan, S. C. , Edwards, P. J., Aggarwal, A., Graca, J., Rietdorf, K., Matchkov, V., Fenton, R. A., Chang, W., Krssak, M., Stewart, A., Broadley, K. J. , Ward, D. T., Price, S. A., Edwards, D. H., Kemp, P. J. and Riccardi, D. 2016. The vascular Ca2+-sensing receptor regulates blood vessel tone and blood pressure. American Journal of Physiology - Cell Physiology 310 (3) , C193-C204. 10.1152/ajpcell.00248.2015

Publishers page: http://dx.doi.org/10.1152/ajpcell.00248.2015

Please note:
Changes made as a result of publishing processes such as copy-editing, formatting and page numbers may not be reflected in this version. For the definitive version of this publication, please refer to the published source. You are advised to consult the publisher's version if you wish to cite this paper.

This version is being made available in accordance with publisher policies. See http://orca.cf.ac.uk/policies.html for usage policies. Copyright and moral rights for publications made available in ORCA are retained by the copyright holders.

The vascular Ca^{2+}-sensing receptor regulates blood vessel tone and blood pressure

M. Schepelmann[1], P.L. Yarova[1], I. Lopez-Fernandez[1,2], T.S. Davies[1], S.C. Brennan[1], P.J. Edwards[1], A. Aggarwal[3], J. Graca[1,4], K. Rietdorf[5], V. Matchkov[6], R.A. Fenton[6], W. Chang[7], M. Krssak[8], A. Stewart[1], K.J. Broadley[9], D.T. Ward[10], S.A. Price[4], D.H. Edwards[11], P.J. Kemp[1] and D. Riccardi[1]

[1]*School of Biosciences, Cardiff University, Museum Avenue, Cardiff CF10 3AX, United Kingdom*
[2]*Faculty of Pharmacy, Université de Picardie Jules Verne, Pôle santé 3, 80036 Amiens, France*
[3]*Department of Pathophysiology and Allergy Research, Medical University of Vienna, 1090, Vienna, Austria*
[4]*Pathology Sciences, AstraZeneca, Alderley Park, Macclesfield, Cheshire, SK10 4TG, United Kingdom*
[5]*Faculty of Science, Department for Life, Health and Chemical Sciences, The Open University, Milton Keynes, MK7 6AA, UK*
[6]*Department of Biomedicine, Aarhus University, Ole Worms Allé, 8000, Aarhus C, Denmark*
[7]*Endocrine Research Unit, Department of Veteran Affairs Medical Center, Department of Medicine, University of California, San Francisco, CA, USA*
[8]*Division of Endocrinology and Metabolism, Department of Medicine III, Medical University of Vienna, 1090, Vienna, Austria*
[9]*School of Pharmacy and Pharmaceutical Sciences, Division of Pharmacology, Cardiff University, King Edward VII Avenue, Cardiff CF10 3XF, United Kingdom*
[10]*Faculty of Life Sciences, University of Manchester, Oxford Road, Manchester M13 9PT, United Kingdom*
[11]*Cardiff University, Wales Heart Research Institute, Cardiff CF14 4XN, United Kingdom*

Corresponding author for final article:
Daniela Riccardi, PhD
Division of Pathophysiology and Repair
Cardiff University, United Kingdom
Telephone: +44 (0) 29 208 79132
Facsimile: +44 (0) 29 208 74116
Email: Riccardi@cf.ac.uk

Corresponding author for production:
Martin Schepelmann, PhD
Division of Pathophysiology and Repair
Cardiff University, United Kingdom
Telephone: +44 (0) 29 208 79069
Facsimile: +44 (0) 29 208 74116
Email: SchepelmannM@cardiff.ac.uk

Contributions:

MS, PY, IL, TD, SCB, PE, KR, AA, VM, DTW, AS performed the experiments
MS, PY, IL, KR, PE analyzed the data
VM, RAF, MK, KB, DHE contributed analytical tools and equipment
WC generated the mouse model
MS, PY, IL, VM, RAF, DHE, DR, PJK designed the research
MS, PY, PJK, DR wrote the manuscript

Running head: The vascular CaSR regulates blood vessel tone

Key words: calcium-sensing receptor, CaSR; vascular smooth muscle cells; blood pressure regulation; G protein-coupled receptor; blood vessel tone regulation

Abstract

The extracellular calcium-sensing receptor, CaSR, is expressed in blood vessels where its role is not completely understood. In this study, we tested the hypothesis that the CaSR expressed in vascular smooth muscle cells (VSMC) is directly involved in regulation of blood pressure and blood vessel tone. Mice with targeted CaSR gene ablation from vascular smooth muscle cells (VSMC) were generated by breeding exon 7 LoxP-CaSR mice with animals in which Cre recombinase is driven by a SM22α promoter (SM22α-Cre). Wire myography performed on Cre-negative (wild-type, WT) and Cre-positive $^{SM22\alpha}CaSR^{\Delta flox/\Delta flox}$ (knock-out, KO) mice showed and endothelium-independent reduction in aorta and mesenteric artery contractility of KO compared to WT mice in response to KCl and to phenylephrine. Increasing extracellular calcium ion (Ca^{2+}) concentrations (1-5 mM) evoked contraction in WT, but only relaxation in KO aortae. Accordingly, diastolic and mean arterial blood pressures of KO animals were significantly reduced compared to WT, as measured by both tail cuff and radiotelemetry. This hypotension was mostly pronounced during the animals' active phase and was not rescued by either NO-synthase inhibition with L-NAME or by a high salt-supplemented diet. KO animals also exhibited cardiac remodeling, bradycardia and reduced spontaneous activity in isolated hearts and cardiomyocyte-like cells. Our findings demonstrate a role for CaSR in the cardiovascular system and suggest that physiologically relevant changes in extracellular Ca^{2+} concentrations could contribute to setting blood vessel tone levels and heart rate by directly acting on the cardiovascular CaSR.

Introduction

The extracellular calcium-sensing receptor, CaSR, was the first G protein-coupled receptor identified that has an ion, Ca^{2+}, as its primary physiological agonist. The CaSR was initially found in the parathyroid glands, where it acts as a controller of free ionized extracellular-Ca^{2+} (Ca^{2+}_o) concentration in the blood via the regulation of parathyroid hormone (PTH) secretion (6). Systemic administration of pharmacological modulators of the CaSR have been shown to affect blood pressure in various animal models (50). However it is unknown whether these effects are due to systemic or local actions of the CaSR. Indeed, the CaSR expression is found in the vasculature (7, 54, 59), but a definitive role for this receptor in blood pressure regulation has never been firmly established. In the vascular endothelium, CaSR activation is thought to stimulate nitric oxide (NO) production (34, 59) and/or endothelium-derived hyperpolarization (EDH) (54). In rat subcutaneous small arteries, Ca^{2+}_o evokes a biphasic response with contraction followed by dilatation in a concentration-dependent manner (40). Furthermore, activation of the endothelial CaSR in mouse aortic segments induces endothelium-dependent and -independent relaxations (34). Alteration in CaSR expression or function in vascular smooth muscle cells (VSMC) has been linked to pathological conditions such as microvascular complications during diabetes (34), vascular calcification (1) and idiopathic pulmonary arterial hypertension (55). Allosteric CaSR activators, termed calcimimetics, have been on the market since 2004 for the treatment of hyperparathyroidism secondary to kidney failure (3). In patients with chronic kidney disease (60), and in a rat model of surgically-induced chronic kidney disease (39), calcimimetic treatment is associated with antihypertensive effects. However, because calcimimetics are phenylalkylamine derivatives, their ability to reduce blood pressure has been ascribed to potential off-target effects on L-type Ca^{2+} channels (37, 52). Given the importance of the CaSR in many physiological processes (43), the aim of this study was to determine whether the CaSR in

VSMC contributes directly to blood pressure regulation. For this purpose, we generated animals with targeted CaSR ablation from smooth muscle cells by breeding mice with LoxP sites flanking exon seven of the CaSR (13) with mice in which Cre recombinase expression is transcriptionally regulated by the SM22α promoter (30). This approach allowed us to study animals with targeted deletion of the CaSR from VSMC throughout the vascular system, visceral smooth muscle and cardiac cells, but not skeletal muscle cells (30, 56).

Materials and Methods

Animals

Commercially available SM22α-Cre$^+$ mice (Jackson Immunoresearch Laboratories, Bar Harbor, ME, USA) were crossed with exon7-LoxP CaSR sites (13). The CaSR-LoxP strain was generated from C57BL/6 x SVJ129 backcrossed with C57BL/6 for 8 generations. CaSR-LoxP x SM22α-Cre mice were inbred for at least 3 generations before being used for experiments. Genotyping for CaSR-LoxP sites and Cre was performed as described elsewhere (13, 25, 56). All animal work was conducted according to UK legislation (Home Office project license 30/3007) and conformed to the guidelines from directive 2010/63/EU of the European Parliament on the protection of animals used for scientific purposes. Euthanasia for tissue collection was performed by cervical dislocation according to UK legislation (A(SP)A 1986, Schedule 1).

Genotyping

DNA from ear biopsies was extracted using DirectPCR® Ear DNA Extraction system (Viagen, Los Angeles, CA, USA) with proteinase K (Bioline, London, UK) according to the manufacturer's instructions. Genotype was determined using the SM22α promoter and Cre coding region primers from (25) and the LoxP primers already described (13). Primer sequences: *SM22-Pro* (CAGACACCGAAGCTACTCTCCTTCC), *SM22-Cre* (CGCATAACCAGTGAAACAGCATTGC), *CaSR fl up* (GTGACGGAAAACATA CTGC), *CaSR fl low* (CGAGTACAGGCTTTGATGC). BioTaq Taq-polymerase (Bioline) was used for polymerase chain reaction (PCR). Final concentrations per reaction: 100 nM per primer, 1 mM dNTPs (Bioline), 4 mM $MgCl_2$, 2 U polymerase, 1.6 % ear lysate. PCR conditions: 5 minutes initial denaturation at 95 °C, 40 cycles of 30 seconds 95 °C, 60 seconds 50 °C (Cre)

or 47 °C (LoxP), 120 seconds 72 °C, and a final elongation of 10 minutes at 4 °C. Amplification products for Cre were visualized using agarose gel electrophoresis with an expected amplicon size of 500 bp in case of at least one Cre-positive allele. Amplification products for LoxP were visualized using polyacrylamide gel-electrophoresis with an expected amplicon size of 167 bp for floxed alleles and 133 bp for non-floxed alleles.

Chemicals and reagents

All chemicals and reagents were obtained from Sigma-Aldrich (Poole, Dorset, UK) and Life Technologies (Paisley, Strathclyde, UK) unless otherwise stated.

Real time reverse transcription PCR (RT-qPCR)

RT-qPCR was performed on endothelium-denuded aortae as described previously (22). Gene expression was calculated based on the $2^{-\Delta\Delta Ct}$ method (33), normalized to the expression of the housekeeping gene β-actin. Samples with Ct values ≥ 31 for pecam-1 were considered to be devoid of endothelial contamination. Primers: *Calcium-sensing receptor exon 6-7 (CaSR6-7)* Fwd: GTGGTGAGACAGATGCGAGT; Rev: GCCAGGAACTCAATCTCCTT. *β-actin* (Fwd: TCCTAGCACCATGAAGATCA; Rev: CCACCGATCCACACAGAGTA), Pecam-1 (Fwd: AGACATGGAATACCAGTGCAGAG; Rev: ACAGGATGGAAATCACAACTTCAT).

Western Blot

CaSR immunoblot of microsomal membrane fractions from endothelium-denuded aortae or lysate from HEK-293 cells stably expressing the human CaSR (positive control) was

performed as described previously (53) using an antibody directed against the amino terminus of the CaSR (Anaspec, Freemont, CA, USA). Expression of α-smooth muscle actin was detected using a mouse monoclonal antibody.

Intracellular calcium imaging

The thoracic aorta was dissected and cleaned in cold DMEM-F12 supplemented with 1% penicillin/streptomycin (Life Technologies, Paisley, U.K.), cut-open for endothelium removal and cut into 1-2mm segments, subsequently incubated for 30 minutes at 37 ºC in 5% CO_2 in an enzymatic digestion solution containing DMEM-F12 supplemented with 1 mg/ml papain, 1mg/ml collagenase from Clostridium histolyticum, 1 mg/ml fatty acid free BSA, 1 mg/ml DTT and 0.5 mg/ml soybean trypsin inhibitor. The cell suspension was seeded onto glass coverslips coated with poly-D-lysine and allowed to settle for 30 minutes at 37 ºC in 5% CO_2, after which cells were incubated for 30 minutes with extracellular solution (135 mM NaCl, 10 mM glucose, 5 mM KCl, 5 mM HEPES, 1.2 mM $MgCl_2$, 1 mM $CaCl_2$, pH 7.4) containing 1.4 μM fura-2 AM, dissolved in DMSO (Life Technologies). $Ca^{2+}{}_i$ recordings were performed as described previously (46).

Wire myography

Wire myography on mouse aortae and MA was performed as described elsewhere (5, 17, 19). In brief, thoracic aortae and second order MA of 4-6 month old mice were carefully dissected in cold buffer (118 mmol/l NaCl, 3.4 mmol/l KCl, 1.2 mmol/l KH_2PO_4, 1.2 mmol/l $MgSO_4$, 25 mmol/l $NaHCO_3$, 11 mmol/l glucose, 1 mmol/l $CaCl_2$, bubbled with 95% O_2/5% CO_2) and cut into 2 mm segments. For the study of vascular responses to the calcimimetic NPS-R-568, the extracellular solution contained 1.5 mM $CaCl_2$. The vessel rings were then carefully

mounted in a wire myograph (Danish MyoTechnology, Aarhus, Denmark) using two gold-plated tungsten wires (d = 25 μm) for MAs, or stainless steel wires (d = 40 μm) for aortas. The vessels were let to equilibrate for 20 min at 37°C, and then gradually stretched (up to 2 mN for mesenteric arteries and 5 mM for aorta). The plateau values after each stretch were used to calculate the lumen diameter that would give a target transmural pressure, which for MAs was set as 70 mmHg, and for aortas - 100 mmHg. After normalization, vessels were left to equilibrate for another 30 min, and tested for viability using phenylephrine (PE) and acetylcholine (ACh). Where stated, the endothelium was removed by gentle rubbing of the vessel lumen with a clean human hair, or an air bubble was pushed through the lumen of the vessel. Lack of relaxation in response to 10 μM ACh was used to confirm the successful endothelial denudation. High KCl (40 mM) was used as an alternative, depolarizing, vasoconstrictor (11, 41, 51). When required, the vessels were pre-treated with Nitro-L-arginine methyl ester (L-NAME) for at least 20 min prior to the experiment, and concentration-response curves were obtained by cumulative addition of rising concentrations of the agonists (PE, ACh, $CaCl_2$ and SNAP) directly to the bath. Solutions were changed every 20 minutes to avoid alterations of osmolarity. In order to calculate the percentage change in contractility of KO vessels in comparison to WT, each contraction data point was normalized to the average of individual maximal contraction values of WT vessels. For the dilatation experiments, vessels were first pre-contracted with PE, and then vasodilators were added to the bath. 0% relaxation is the level of tension before the vasorelaxant agonist was added, and 100% relaxation reflects the return of the tension to the basal level.

Tail cuff and radiotelemetry measurements

Blood pressure of male, age-matched animals (4-9 months) were measured by tail cuff on awake, conscious animals during day-time using a 2-channel CODA system (Kent Scientific,

Torrington, CT, USA), following the manufacturer's instructions and using 20 acclimatization and 10 measurement cycles.

Radiotelemetry was performed on 3 month old mice using implantable probes with HD-X11 transmitters (4). Mice were anesthetized by subcutaneous injections with a combination of fluanisone (10 mg/kg body weight), fentanyl (0.3 mg/kg body weight) and midazolam (1 mg/kg body weight) and placed in dorsal recumbence on a thermostatically controlled heating platform for maintaining body temperature at 37.5°C. The body hair was liberally removed from the skin on the neck and the skin was disinfected by isopropyl alcohol. A 1–1.5 cm long midline incision through the skin on the neck was made and the mandibular glands were carefully separated. The carotid artery along the left side of the trachea was carefully isolated with fine–tipped forceps from the surrounding tissues. The distal side of the carotid artery (just before the bifurcation) was occluded permanently with 6-0 non-absorbable suture and another suture was placed proximately for temporal occlusion of blood flow to allow for placement of the catheter. Additional suture was placed in the middle to hold the catheter in place after the cannulation of the artery. The artery was pierced using the 25-gauge bent needle just proximately the permanent ligation suture and the catheter was inserted into the vessel using Vessel Cannulation Forceps (Data Sciences International, USA). The catheter was advanced into the artery until it reaches the occlusion suture, the loose middle suture was tightened and occlusion suture released. The catheter was then advanced further until the sensing region was positioned in the aortic arch. The occlusion suture was tightened and a subcutaneous pocket was made by inserting small surgical scissors. A HD-X11 radiotelemetry transmitter (Data Sciences International, USA) was then placed in the pocket. The terminal end of the positive lead was positioned with a small hemostat subcutaneously from the neck incision to the left caudal rib region (approximately 1 cm to the left of the xyphoid process). The negative lead terminal end was positioned with a small hemostat subcutaneously from the neck incision to the right pectoral muscle. The skin incision was closed using 6-0 non-

absorbable suture. Painkiller (0.2 ml/kg; Temgesic, Schering-Plough Europe, Belgium) was injected subcutaneously at the end of operation. Mice were allowed to recover for 2 days before housing them in metabolic cages where they were kept on control diet for 4 days. The standard (control) diet was then changed to a high salt diet (containing 4% NaCl) for a period of 5 days. For reasons of animal welfare, mice were then transferred back in normal housing cages and kept on standard diet for a washout period of 3 days, after which drinking water of the mice was supplemented with 0.5 g / L L-nitro-arginine-methyl-ester (L-NAME).

Telemetry signals from the probes were recorded for the whole duration of the experiment in intervals of 5 minutes in quintuplicates resulting in 60 measurements per hour. Registration was performed with Dataquest A.R.T™ software 4.3. Analyses were performed with Ponemah analyses software 5.00 (all Data Sciences International, USA) and Microsoft Excel 2010. Raw values were concentrated to hourly datapoints. For statistical analysis, three hour intervals of the raw data were averaged for night-time (active phase, 20:00-23:00) and day-time (resting phase, 8:00-11:00). The standard diet vs. high salt diet and standard diet vs. 0.5 g / L L-NAME diet phases were treated as two separate experiments because of the different housing conditions. For graphical representation only, traces were calculated as rolling average over 4 hours.

Cardiac cine-MRI

Cardiac cine-MRI (magnetic resonance imaging) scans of aged (14 month old) mice were acquired using a Bruker Biospec 94/20 9.4 Tesla small bore (20 cm) MRI spectrometer equipped with S116 high performance gradient insert and Avance II electronics (Bruker, Ettlingen Germany). Scans were acquired using a 72 mm transmit/receive quadrature polarized birdcage coil. Mice were kept under general anesthesia using 1-5 % isoflurane in a 40% O_2 / air at 1.2 L / min during scanning. Animals were ECG, respiration and temperature

monitored using a Model 1025 monitoring and gating system (SAIInc, Stony Brook, New York, USA). The temperature of the animals was kept at 37 °C using temperature controlled bath feeding into the restraining scaffold. T2 weighted, respiratory and cardiac gated, fast-imaging with steady-state precession pro-cine scans were performed with a field of view of 32 × 32 mm, an echo time of 1.228 ms, a repetition time of 5 ms, a band width of 125 kHz and slice thickness of 1-1.5 mm were collected from apex to the aortic arch using Paravision 5.0 (Bruker). Gating was performed using using the Small Animal Monitor software and monitoring equipment according to the manufacturer's instructions (SA Instruments, Stony Brook, NY, USA). Scans performed for each mouse included Tri-axial pilot orientation scan, central long-axis cine-scan, short axis cine-scans coving sub-apical to supra-basal image plane. Scans were analyzed using the academic version of Segment 1.9 R2626 (http://segment.heiberg.se) (21) by one person blinded to the genotype of the animals. Functional parameters were assessed from multi-slice short-axes cine MR images by manual markup of left-ventricular endocardium and epicardium in the first timeframe of the slice showing the papillary muscles. The markup was then propagated in time and adjusted to fit the new timeframe. After the markup of the slice was completed, the markup for the whole cine-cycle was propagated apically and basally and contours were again adjusted to fit the respective scans. End-diastole and -systole were defined as the timeframe showing highest and lowest ventricular volume using the auto-detection feature of the Segment software. For wall thickness measurements, the thicknesses of the second and third apical slice in end-systole and -diastole, measured with the respective tool in the Segment software, were averaged. Based on the long axis scans, hearts of KO animals showing full apical end-systolic closure were selected as remodeled sub-group.

Histomorphology and fibrosis staining

Sections from paraffin-embedded hearts and aortae were stained with haematoxylin and eosin (H&E). To detect fibrosis in heart sections of aged mice, collagen deposition was visualized in 8 µm cryosections of paraformaldehyde-fixed hearts stained with picrosirius-red mixture. 8 µm cryosections of paraformaldehyde-fixed (4% in phosphate buffer saline (PBS) for 4 hours) hearts of adult mice were thawed in PBS-T (0.1% Tween-20) for 20 minutes and washed in distilled water for 2 minutes. Sections were then pre-stained with 0.1% fast green for 15 minutes, washed twice in 1 % acetic acid for 15 seconds, washed in distilled water for 2 minutes. Final staining was achieved by incubation in a solution of 0.1 % fast green, 0.1% direct red and 1.3 % picric acid for 1 hour. Sections were then washed three times in 1 % acetic acid for 15 seconds and distilled water for 2 minutes and finally dehydrated in rising concentrations of ethanol, cleared in xylene and mounted in DPX:Xylene 4:1, resulting in green staining for all tissues and red staining for fibrotic tissue. Fibrotic area was quantified using CellProfiler 2.1.1 (28) by one person blinded to the genotype of the animals. All epicardial and endocardial positive (red) staining was manually removed along with other image artefacts (e.g. tissue folding). An image analysis pipeline was run to separate different shades of red pixels (fibrosis positive) from background tissue (green). Cardiac fibrosis percentage was calculated by dividing the number of detected red pixels per 100 positively stained pixels (red + green).

Ex vivo measurement of baseline heart rate

Rapidly dissected hearts were retrogradely perfused in Langendorff fashion. Baseline heart rates were measured using longitudinal force tonometry (31). 6 month old male mice were killed by cervical dislocation. The thorax was rapidly opened and the heart, lungs and thoracic aorta removed to ice cold Krebs buffer (118 mmol / L NaCl, 3.4 mmol / L KCl, 1.2 mmol / L

KH_2PO_4, 1.2 mmol / L $MgSO_4$, 25 mmol / L $NaHCO_3$, 11 mmol / L glucose, 1 mmol / L $CaCl_2$). The aorta was cannulated with a gauge 20 hypodermic needle filled with Krebs buffer and the tip of the needle was advanced to the aortic valve. The needle was attached to the perfusion apparatus and the heart perfused in Langendorff mode (31) at a constant flow rate of 3 ml/min (Gilson Minipuls 3 peristaltic pump, Gilson, Luton, UK) with warmed (37.5°C) Krebs buffer pregassed with O_2/CO_2 (95%/5%). Coronary perfusion pressure was measured by means of a pressure transducer (MLT 844, ADInstruments, Chalgrove, UK) located immediately before the warming coil, where a Condon mercury manometer was also located to accommodate perfusion fluid during pressure changes. A clip was attached to the apex of the heart and linked via a thread and pulley to an isometric tension transducer (50g sensitivity range) (ADInstruments) for measuring contractile tension. A resting diastolic tension of 2g was applied at the start of the experiment and readjusted periodically. The heart was surrounded by a heated jacket (37.5 °C). Isometric cardiac contractions were recorded by means of a Powerlab 8/30, Chart 5, data acquisition system (ADInstruments) and heart rate was derived from the cardiac contractions signals.

Spontaneous activity of PVC in lung slices

Murine lung slices were prepared as described previously (44). In brief, 4-6 month old mice were killed by cervical dislocation and, after opening of the chest cavity, the trachea was cannulated and lungs were inflated by injecting ~ 1.2 ml of low melting point agarose (37 °C, 1.8 % in sHBSS; Life Technologies, Paisley UK). The agarose was stiffened by applying cold sHBSS supplemented with 20 mM HEPES, pH 7.3) over the lungs. The stiffened lungs were cut into ~ 180 µm thick slices using a Vf-300 microtome (Precisionary Instruments, Greenville, NC, USA). Slices were kept in a humidified cell culture incubator with 5 % CO_2 in DMEM:F12 (Life Technologies), supplemented with 10 % FBS. Slices were loaded in the

dark with 20 μM Oregon-Green BAPTA-1 AM (Life Technologies) in the presence of 0.1 % Pluronic F127 (Life Technologies) and 200 μM sulfobromophtalein in sHBSS at room temperature for one hour, followed by de-esterification for at least 30 minutes in the dark in sHBSS with 200 μM sulfobromophtalein. Slices were then mounted in a custom-built imaging chamber and imaged on a Nikon Eclipse Ti microscope, using a Nikon S Fluor 40x oil immersion objective, with an excitation of 470 ± 15 nm. Emission was measured at 525± 25 nm. Images were acquired with a frame rate of 25 frames per second using OptoFluor software (Cairn Research, Faversham, U.K.). Image acquisition was performed for ~ 20 s periods to record the frequency of the spontaneous activity. Image analysis was performed using ImageJ software (47).

Statistical analyses

Statistical analyses were performed using GraphPad Prism 6.04 (GraphPad Software, La Jolla, CA, USA). Statistical tests employed are stated with the respective results or in the figure legends. Where two curves were compared, asterisks (*) above individual data points indicate point-by-point comparison by Holm-Sidak post-test of two-way ANOVA; plus-signs (+) indicate difference of the fitted curves by extra sum-of-squares F test and two-way ANOVA. N states the number of individual biological repeats (number of animals, cell batches, etc.).

Results

Generation of $^{SM22\alpha}CaSR^{\Delta flox/\Delta flox}$ mice

Breeding of SM22α-Cre^{+} mice with mice in which LoxP sites flanked exon 7 of the CaSR gene (LoxP-CaSR$^{+/+}$) (13) yielded $^{SM22\alpha}CaSR^{\Delta flox/\Delta flox}$ mice (which were termed “knockout”,

"KO"). Age- and sex-matched mice expressing only floxed CaSR alleles but no Cre-recombinase (SM22α-Cre$^{-/-}$-LoxP-CaSR$^{+/+}$) were used as controls for all experiments (termed wild-type, "WT"). The resulting truncated Δexon7 product was shown to be non-functional (13) and these animals are viable and fertile (56). Representative genotyping is shown in **Figure 1A**. Aortae of KO animals appeared histomorphologically normal and indistinguishable from those of WT mice of comparable ages (**Figure 1B**), suggesting that CaSR deletion does not affect the histomorphology of blood vessels.

Molecular and functional CaSR expression in the vasculature was found to be significantly reduced in KO compared to WT animals. *Bona fide*, CaSR-like immunoreactivity, corresponding to the molecular mass of the fully mature dimeric form of the receptor, (53) was reduced in membrane fractions from endothelium-denuded KO aortae compared to that seen in WT, as shown by western blot using a polyclonal antibody that preferentially detects the dimeric form of the CaSR. CaSR deletion from VSMC did not affect the expression levels of α-smooth muscle actin (**Figure 1C**). RT-qPCR carried out in endothelium- and adventitia denuded aortae from WT and KO animals showed that expression of the CaSR (exon 6-7) was significantly reduced in KO vessels compared to WT (**Figure 1D**). Classically, CaSR activation is linked to phosphoinositide turnover and an increase in intracellular Ca^{2+} concentration ($[Ca^{2+}]_i$) (6). In fura-2 loaded VSMC isolated from WT and KO mouse aortae, increasing $[Ca^{2+}]_o$ from 0.1 to 5 mmol / L evoked a concentration-dependent increase in $[Ca^{2+}]_i$ in WT VSMC, which was significantly smaller in KO VSMC (**Figure 1E**).

Ex vivo blood vessel contractility is impaired in $^{SM22\alpha}CaSR^{\Delta flox/\Delta flox}$ mice

Previous studies have suggested a role for the CaSR in vascular tone regulation (50). To test this hypothesis directly, we performed *ex vivo* tension measurements on isolated aortae and mesenteric arteries (MA) from WT and KO mice. Rings of aortae and MA of KO animals

showed a significantly smaller contraction in response to a depolarizing stimulus (*i.e.* high K^+) compared to aortic rings from WT (**Figure 2A and 2B**). A comparable level of reduction in KO aortae and MA contractility was observed when phenylephrine (PE, 1 nmol / L – 30 μmol / L), an agonist of the $G_{q/11}$ protein-coupled α_1-adrenoceptor, was employed (**Figure 2C and 2D**). Except for the responses to PE, where potency was slightly but significantly reduced in KO aortae and MA compared to WT control, EC_{50} values in all other experiments remained unchanged (**Table 1**). In contrast, endothelium-dependent relaxation of PE-precontracted blood vessels in response to acetylcholine (ACh) was modestly, but significantly enhanced in KO aortae (**Figure 2E**), and reduced in KO MA (**Figure 2F**).

In line with this reduction in contractility in response to contractile stimuli, we observed a reduction in Ca^{2+}_i signaling in VSMC isolated from KO mice compared to WT cells in the presence of depolarizing concentrations of K^+ (60 mmol / L KCl, KO vs WT: 3.81 ± 0.62 *vs.* 1.90 ± 0.53 fold *vs.* baseline, N = 5, $p < 0.05$, Student's t-test).

To investigate the effects of the physiological CaSR agonist, Ca^{2+}_o, on the vascular tone, we precontracted aortae and MA from WT and KO animals with PE to approximately 60% of maximal tone, and then cumulatively added rising concentrations of Ca^{2+}_o (from 1 to 5 mmol / L). Aortae of WT animals displayed significantly different response to Ca^{2+}_o than aortae from KO animals, showing a moderate contraction to Ca^{2+}_o that reached 19.9 ± 7.8 % at 2.5 mmol / L Ca^{2+}_o: ($p < 0.05$, one sample t test *vs* baseline), whilst aortae from KO animals showed only relaxation that reached 33.4 ± 11.8 % in the presence of 4 mmol / L Ca^{2+}_o ($p < 0.05$, one sample t test *vs* baseline; **Figure 2G**). In contrast, MA displayed only relaxation to rising $[Ca^{2+}]_o$ that was of comparable magnitude in vessels from WT and KO animals (**Figure 2H**). In order to determine CaSR specificity of the responses observed in the aortae, aortic rings were preconstricted with PE to ~ 60% of maximal tone, and then treated with increasing concentrations of the calcimimetic NPS R-568 (10 nM-10 μM). NPS R-568 evoked

contraction followed by relaxation in WT aortae while KO aortae were insensitive to low concentrations of calcimimetic (10 nM – 300 nM) and only responded with vasodilation at concentrations higher than 1 μM NPS R-568 (Figure 3A). After removal of the endothelium, aortae from WT mice still showed a contractile response to rising concentrations of NPS R-568 but did not show any relaxation even at very high levels of the calcimimetic. Endothelium denuded aortae from KO animals were completely insensitive to NPS R-568 (Figure 3B).

Inhibition of nitric oxide synthase (NOS) with NG-nitro-L-arginine methyl ester (L-NAME) (100 μmol / L) (**Figure 4A and B**) or endothelial denudation (**Figure 4C and D**) did not abolish the reduction in contractility in KO aortae and MA compared to WT. These results indicate that the impaired vascular contractility observed in KO animals was not due to an increase in endothelium-mediated relaxation. Abrogation of NO signaling with L-NAME led to ACh-induced contraction (16, 27, 42) in both WT and KO aortae which again was significantly smaller in aortae from KO animals compared to WT **(Figure 4E,** negative relaxation = contraction**)**. In MA, L-NAME abrogated the differences in the relaxation response to ACh between KO and WT (**Figure 4F**). Endothelium-independent relaxation following treatment with the NO donor S-Nitroso-N-acetylpenicillamine (SNAP; 1 nmol / L – 30 μmol / L) showed no difference in ACh sensitivity between WT and KO endothelium-denuded aortae and MA (**Figure 4G and H**). EC_{50} values of all agonists in these series of experiments were unchanged between WT and KO animals (**Table 1**).

$^{SM22\alpha}CaSR^{\Delta flox/\Delta flox}$ mice are hypotensive

The impaired vascular contractility of KO mice suggested an effect of VSMC-CaSR deletion on blood pressure *in vivo*; and indeed, tail cuff measurements in adult male mice showed that KO animals exhibited a reduction in blood pressure (approximately 5% systolic, 9% diastolic and 7% mean arterial pressure, MAP) compared to the WT (**Figure 5A-C**). Longitudinal

radiotelemetry experiments confirmed this reduction in systolic and diastolic blood pressure and MAP. Notably, this reduction was only apparent during night-time, when the animals were active, but not during day-time when the animals were resting. Short-term L-NAME treatment (38) increased blood pressure in animals of both genotypes but did not abolish the hypotension of KO relative to WT mice (**Figure 5D-F and Table 2**). Pulse height was increased in KO animals compared to WT mice (**Figure 5G**), particularly following L-NAME treatment, owing to the bigger difference in diastolic than systolic pressures between the genotypes. Short-term dietary NaCl supplementation yielded no changes in systolic or diastolic blood pressure in either WT or KO animals (**Table 2**).

$^{SM22\alpha}CaSR^{\Delta flox/\Delta flox}$ mice are bradycardic

In addition to the impaired vascular reactivity that is associated with hypotension in the $^{SM22\alpha}CaSR^{\Delta flox/\Delta flox}$ mice**,** radiotelemetry experiments also revealed that heart rates of these animals were about 5 % (day-time) to 17% (night-time) below those of WT mice (**Figure 6A and Table 2**). Furthermore, during night-time, the positive first derivative of the blood pressure curve (dp/dt), an indirect measure of inotropy (36), was significantly higher in the KO compared to WT mice. Short-term L-NAME treatment, while decreasing heart rate in mice of both genotypes, did not affect the difference in heart rates between WT and KO animals nor did it influence dp/dt in these animals (**Figure 6B and Table 2**). A high salt diet led to a small reduction in heart rate of WT and KO animals during day-time and did not affect dp/dt (**Table 2)**.

$^{SM22\alpha}CaSR^{\Delta flox/\Delta flox}$ mice exhibit cardiac remodeling

The observed bradycardia presented by the KO mice could be accounted for, at least in part, by direct CaSR ablation from cardiomyocytes as the SM22α promotor has been shown to

direct Cre expression transiently to the heart (30). This consideration, together with recent evidence suggesting that the CaSR plays a role in electromechanical coupling of cardiomyocytes (48), led us to investigate more thoroughly the cardiac phenotype of $^{SM22\alpha}CaSR^{\Delta flox/\Delta flox}$ mice. While there were no differences between hearts from WT and KO animals by superficial observation or any histomorphological changes seen by H&E staining (**Figure 7A**), KO animals showed a reduction in fibrosis when compared to age-matched WT controls (**Figure 7B**) (0.93 ± 0.08 *vs.* 2.09 ± 0.43 % fibrotic area, N = 9 (KO), 10 (WT), $p < 0.05$, Student's t-test with Welch's correction).

Cardiac cine-MRI showed that the long axes of WT and KO hearts of aged animals were comparable between genotypes in end-diastole but presented with a visible difference in end-systole in hearts from 5 out of 11 investigated KO animals. In these hearts, complete closure of the apical left ventricular cavity (2nd apical short-axis MRI slice) was seen, while it was still visible at the end-systole of the hearts of WT mice (**Figure 7C, Video S1**). These functional differences can be easily observed in morphological 3D reconstructions of the left ventricle endocardium (**Figure 7D**). These 5 hearts were thus termed "remodeled" and analyzed as a separate group. MRI analysis showed that left ventricular mass (**Figure 7E**), left ventricular end-diastolic volume (**Figure 7F**) and end end-diastolic volume (**Figure 7G**) and stroke volume (**Figure 7H**) were unaltered between WT and remodeled KO hearts. An observed decrease in end-systolic volume did not reach statistical significance. Ejection fraction (**Figure 7I**), end-diastolic remodeling index (**Figure 7J**, size of the ventricle *vs.* the end-diastolic volume) and wall thickening (**Figure 7K**) were increased in remodeled hearts from KO mice compared to WT hearts.

To test more directly the hypothesis that direct CaSR ablation from cardiomyocytes was responsible for the observed bradycardia in the $^{SM22\alpha}CaSR^{\Delta flox/\Delta flox}$ mouse, we also investigated the base frequency of non-paced hearts from WT and KO mice *ex vivo* in the

absence of autonomic regulation in a retrogradely perfused Langendorff preparation (31). Isolated hearts from KO animals showed a significantly reduced basal heart rate compared to that measured in the hearts of WT animals (**Figure 7L**), suggesting that CaSR deletion from the heart has a direct impact on chronotropy. Pacemaker activity also occurs in the pulmonary veins, which contain cardiomyocyte-like pulmonary vein sleeve cells (PVCs). PVCs employ the same electrochemical coupling machinery as atrial cardiomyocytes (14), can act as pacemaker cells (12, 26, 57) and can be easily studied in *ex vivo* lung slice preparations as they are present in the murine lung. In PVCs from KO animals, there was a reduced rate of spontaneous activity, measured as changes in $Ca^{2+}{}_{i}$ compared to WT mice (KO vs WT: 0.58 ± 0.10 vs 1.00 ± 0.09 fold, N = 6, $p < 0.05$, Student's t-test), suggesting that the bradycardia is an intrinsic feature of the KO animals.

Discussion

Vascular phenotype

$^{SM22\alpha}CaSR^{\Delta flox/\Delta flox}$ mice show changes in their cardiovascular system: the main findings of this study are that $^{SM22\alpha}CaSR^{\Delta flox/\Delta flox}$ mice exhibit impaired vasoconstriction, systemic hypotension and bradycardia.

Ex vivo tension measurements of aortae and mesenteric arteries from WT and KO mice demonstrated impaired contractile responses to high K^+, (a depolarising stimulus) and impaired maximum contractility in response to PE (GPCR-mediated). In addition, the potency of PE to contract KO blood vessels was also impaired. These findings indicate that the CaSR sensitizes the response of blood vessels to contractile stimuli. Importantly, no histological difference was found between blood vessels from WT and KO mice, indicating that changes in vessel morphology were not responsible for the observed changes in blood vessel contractility. Furthermore, the reduction in maximum contractility was independent of inhibition of NOS or endothelial denudation while vascular relaxation in response to an exogenous NO donor remained unchanged. In addition, inhibition of NOS signaling can unmask the effects of endothelium-derived contracting factors released from the endothelium upon stimulation that in the absence of NO can cause pronounced vasoconstriction (16, 27, 42). This contractile effect of ACh in the presence of L-NAME was reduced in KO compared to WT aortae, providing yet another indication that the impaired contractility of blood vessels lacking the VSMC CaSR is independent of the contractile stimulus.

Despite the fact that the sensitivity to an NO donor was comparable in WT and KO vessels, the endothelium-dependent relaxation was differentially affected in MA and aortae. ACh evoked enhanced relaxation in KO aortae which may be explained by the aforementioned reduced contractile component of the ACh response. KO MAs, in contrast, exhibited a small

but significant suppression of the ACh-mediated relaxation that was absent when L-NAME was added. These findings suggest a reduced endothelium-derived NO signalling in MA, as induced by endothelial stimulation (e.g. ACh), while the sensitivity of VSMC to NO itself was unaffected in KO animals.

In line with our results of genetic ablation, Loot and colleagues have recently found that pharmacological inhibition of the CaSR attenuated vascular contraction in response to PE and high K^+ (34). The congruence of these results of pharmacological CaSR inhibition in wild type mice and CaSR ablation in genetically altered mice provides another line of evidence that the VSMC-CaSR is indeed directly responsible for the modulation of vascular tone, rather than possible off-target effects of calcilytic drugs (35) or unexpected side-effects of the genetic ablation. This contractility-enhancing effect of the CaSR is not limited to VSMC, since, using the same animal model as the one we have used for the current studies, we have recently reported that airways of KO mice showed a reduction in contractility in response to the muscarinic ACh receptor agonist methacholine when compared to WT mice (56), similarly to the observed reduction in blood vessel contractility in response to PE in this study. Finally, the observed effects in $^{SM22\alpha}CaSR^{\Delta flox/\Delta flox}$ mice were unlikely to be due to impaired SM22α function, as constitutive ablation of SM22α was shown to lead to increased MA vasoconstriction in response to an α_1-adrenoceptor agonist (58). In the current study, the CaSR agonist, Ca^{2+}_o, induced vasorelaxation in WT and KO MA and KO aortae, likely due to stimulation of the endothelial CaSR (34, 54, 59). However, in WT aortae, we observed Ca^{2+}_o concentration-dependent vasoconstriction. These effects of increasing Ca^{2+}_o concentrations inducing vasoconstriction in WT aortae are consistent with previous findings by Ohanian and colleagues (40), who reported vasoconstriction in response to physiological Ca^{2+}_o concentrations in rat subcutaneous small arteries. These authors suggested that the contractile effect was not CaSR-mediated. Similary, Loot and colleagues have reported vascular contraction in response to rising concentrations of Ca^{2+}_o in endothelium denuded or L-NAME

treated mouse aortic rings (34) Here, we have demonstrated that the contracting component of th.e Ca^{2+}_o response was lost in KO aortae. Similarly, airways of WT mice have been shown to react with robust contraction to rising concentrations of the CaSR agonists, Ca^{2+}_o and spermine, and this contractile response was completely lost in airways from animals lacking the CaSR in smooth muscle cells (56). Moreover, results obtained by treating PE-preconstricted aortae with the calcimimetic NPS-R-568 mimicked the results observed by using Ca^{2+}_o to modulate vascular tone. The calcimimetic-mediated contraction in WT aortae was endothelium independent, further corroborating a role for the VSMC CaSR in vessel contractility. Together, these results clearly support the idea that the CaSR mediates Ca^{2+}_o-induced contractions in smooth muscle cells. Cultured VSMC of KO animals reacted with impaired Ca^{2+}_i mobilization to stimulation with both Ca^{2+}_o and K^+, indicating Ca^{2+}_i-signalling as one mechanism of action by which the CaSR affects blood vessel tone. Together, these results demonstrate that the observed impaired vascular contractility in blood vessels of $^{SM22\alpha}CaSR^{\Delta flox/\Delta flox}$ mice, as shown by reduced responses to primary contractile stimuli, is an effect, which is independent of the endothelium and dependent on VSMC CaSR.

Tail cuff and radiotelemetry measurements confirmed the hypotensive phenotype of $^{SM22\alpha}CaSR^{\Delta flox/\Delta flox}$ animals which was predicted from the *ex vivo* vessel tone studies. In both circumstances, we observed a significant reduction in diastolic blood pressure and MAP. This reduction was more apparent during the animals' active than resting phase, suggesting that the modulating effect of the CaSR on blood pressure is dependent on sympathetic activity, again supporting the idea that the effects of the CaSR on blood vessel tone and blood pressure are dependent on the presence of other contractile, or activating, stimuli. A contribution of the cardiac phenotype of the animals, i.e. the reduction in heart rate, to the observed hypotension in $^{SM22\alpha}CaSR^{\Delta flox/\Delta flox}$ animals is likely, although the stronger reduction in diastolic than systolic blood pressure points to peripheral resistance being the principal cause of the hypotension in KO animals.

Acute L-NAME treatment did not abolish this difference in WT and KO mice' diastolic blood pressure, mirroring the aforementioned *ex vivo* results on isolated blood vessels, where NOS-inhibition or endothelial denudation did not abolish the impaired vascular contractility either. This rules out the possibility that, at least in the short-term, the difference in blood pressure between WT and KO mice might be NO-driven. Short-term exposure to a high salt-supplemented diet has been shown to rescue the loss of angiotensin converting enzyme-induced hypotension in mice of a similar background (9). However, the lack of any change in blood pressure in KO animals kept on a high salt diet here suggests that the kidney is not likely to be involved in causing the observed hypotension in our strain.

Pulse height was increased in KO animals following L-NAME treatment. While elevated pulse height is recognized as being a feature of increased arterial stiffening, reduced blood vessel compliance is also accompanied by isolated systolic hypertension in humans and animals (15, 18), which clearly is not the case in KO animals. Indeed, the increased pulse height can be attributed solely to the greater reduction in diastolic than systolic blood pressure in KO animals. In KO animals, L-NAME treatment induced a larger increase in systolic blood pressure (and, therefore, pulse height) than diastolic blood pressure. It is known that the importance of endothelium-dependent NO signaling declines with the reduction of arterial size and plays a major role in aorta and other big arteries, while endothelium-dependent hyperpolarization plays a major role in smaller resistance arteries (49). Therefore, the observed increase in systolic blood pressure in KO mice could be ascribed to NO synthase inhibition having a greater effect in the large conduit arteries, than in resistance arteries (45). Furthermore, L-NAME administration in the drinking water led to a reduction in heart rate of KO animals which was comparable to that observed in WT animals. These results suggest the existence of an intact baroreflex response to the increase in peripheral resistance, or at least that the response of the cardiovascular system to systemic NO synthesis inhibition is not dependent on the VSMC-CaSR.

Collectively, the observations described herein support the hypothesis that the loss of the CaSR from VSMC leads to a reduction of vascular tone, manifesting *in vivo* as a reduction in diastolic blood pressure, which is dependent on the physical activity of the mice. The presence of both a cardiac as well as vascular phenotype in these animals suggests that the observed hypotensive phenotype is likely to be accounted for by a combination of CaSR ablation from both cardiac and vascular systems and further studies are required to dissect these effects in greater detail using cell-specific gene ablation studies in which Cre recombinase is driven by alternative promoters.

It has long been established that the CaSR can translate even minute changes in $[Ca^{2+}]_o$ into intracellular responses (6). These changes in extracellular $[Ca^{2+}]_o$ can also be elicited by extrusion of $[Ca^{2+}]_i$ – indeed, excitation and subsequent extrusion of $[Ca^{2+}]_i$ into the intracellular space has been conclusively demonstrated to activate the CaSR on neighboring cells and elicit intracellular responses in a paracrine fashion, acting in a way as a "third messenger" (10, 23, 24, 29). On the basis of our observations in this study and the aforementioned considerations, we therefore propose a hypothesis of how the VSMC-CaSR and endothelial-CaSR could directly contribute to the maintenance of blood vessel tone (**Figure 8**). A contractile stimulus, *e.g.* via depolarization or α_1-adrenoceptor agonists, leads to an increase in $Ca^{2+}{}_i$ concentration in VSMC. Restoration of normal resting $Ca^{2+}{}_i$ levels is achieved in part via extrusion of $Ca^{2+}{}_i$ into the interstitium, where it is feasible that such localized increase in $Ca^{2+}{}_o$ would activate the VSMC-CaSR in an auto-/paracrine fashion, thus causing potentiation of contraction. Loss of such a mechanism in the $^{SM22\alpha}CaSR^{\Delta flox/\Delta flox}$ mice could account for the observed reduction in VSMC contractility, thus leading to the observed *in vivo* hypotension. This role of the CaSR as modulator of VSMC contractility is further supported by the fact that, conversely, *increased* expression of the CaSR and an associated increase in $[Ca^{2+}]_i$ have been reported in pulmonary arterial smooth muscle cells from patients

with pulmonary arterial hypertension and surrogate animal models (55) which is alleviated by pharmacological CaSR inhibition (20),

Cardiac phenotype

CaSR ablation from SM22α-positive tissues also leads to its deletion from the developing heart (30), which could account for the aforementioned bradycardia in KO mice. Therefore, direct loss of the CaSR from the heart could impact negatively on pacemaker frequency or intracellular coupling. Previously it has been demonstrated in ventricular cardiomyocytes that CaSR activation leads to increased Ca^{2+}_{i} signaling and increased cell shortening culminating in a positive inotropic effect and modification of their electromechanical coupling (48). Isolated *ex vivo* hearts recapitulated the reduction in heart rate observed by radiotelemetry *in vivo*. Indeed, isolated PVC from KO mice, which show similar electrophysiological hallmarks of cardiac pacemaker cells (12, 14, 26, 57), also exhibited reduced lower spontaneous activity than cells isolated from WT miceresults suggesting that the observed bradycardia in KO mice could be ascribed to decreased pacemaker activity. The observed cardiac remodelling, *i.e.* stronger mode of contraction, together with the increase in dp/dt, could thus be interpreted as compensatory response to the bradycardic and hypotensive phenotype. The reduction in fibrosis suggests that KO animals might be protected against the development of age-related cardiac fibrosis (2), maybe via a beneficial effect of their reduced heart rate (8) but could also be a direct consequence of CaSR deletion from the heart, as recently indicated in a rat model of cardiac hypertrophy (32). Further studies will be necessary to completely elucidate the role of the cardiac CaSR.

Conclusions

Taken together, our studies highlight a physiological role for the CaSR in the cardiovascular system. In VSMC, CaSR-mediated regulation of contraction contributes to vessel contractility. Loss of this mechanism, likely together with direct cardiac effects, could account for the observed hypotension in $^{SM22A}CaSR^{\Delta flox/\Delta flox}$ mice. The net balance between the effects of the CaSR in smooth muscle (pro-contractile) and the endothelium (pro-relaxing) determines the influence of the vascular CaSR on vascular tone regulation. Furthermore, KO mice exhibit both *in vivo* and *ex vivo* bradycardia, linking the CaSR to direct modulation of cardiac function. The results of our present study thus implicate the CaSR directly in the local regulation of the cardiovascular system.

Acknowledgements

This work was supported by the European Union though a Marie Curie Initial Training Network ("Multifaceted CaSR", 264663, to DR, PJK and SAP), Amgen, Inc. (to DR), The Novo Nordisk Foundation (to VM), the US Department of Veterans Affairs Merit Review Grant (1I01BX001960, to WC), and the Danish Medical Research Council (to RAF).

Disclosures / Conflict of interest

None declared

References

1. **Alam MU, Kirton JP, Wilkinson FL, Towers E, Sinha S, Rouhi M, Vizard TN, Sage AP, Martin D, Ward DT, Alexander MY, Riccardi D, and Canfield AE.** Calcification is associated with loss of functional calcium-sensing receptor in vascular smooth muscle cells. *Cardiovasc Res* 81: 260-268, 2009.
2. **Biernacka A and Frangogiannis NG.** Aging and Cardiac Fibrosis. *Aging Dis* 2: 158-173, 2011.
3. **Block GA, Martin KJ, de Francisco AL, Turner SA, Avram MM, Suranyi MG, Hercz G, Cunningham J, Abu-Alfa AK, Messa P, Coyne DW, Locatelli F, Cohen RM, Evenepoel P, Moe SM, Fournier A, Braun J, McCary LC, Zani VJ, Olson KA, Drueke TB, and Goodman WG.** Cinacalcet for secondary hyperparathyroidism in patients receiving hemodialysis. *N Engl J Med* 350: 1516-1525, 2004.
4. **Boedtkjer E, Praetorius J, Matchkov VV, Stankevicius E, Mogensen S, Fuchtbauer AC, Simonsen U, Fuchtbauer EM, and Aalkjaer C.** Disruption of Na^+,HCO_3^- cotransporter NBCn1 (slc4a7) inhibits NO-mediated vasorelaxation, smooth muscle Ca^{2+} sensitivity, and hypertension development in mice. *Circulation* 124: 1819-1829, 2011.
5. **Broegger T, Jacobsen JC, Secher Dam V, Boedtkjer DM, Kold-Petersen H, Pedersen FS, Aalkjaer C, and Matchkov VV.** Bestrophin is important for the rhythmic but not the tonic contraction in rat mesenteric small arteries. *Cardiovasc Res* 91: 685-693, 2011.
6. **Brown EM, Gamba G, Riccardi D, Lombardi M, Butters R, Kifor O, Sun A, Hediger MA, Lytton J, and Hebert SC.** Cloning and characterization of an extracellular Ca(2+)-sensing receptor from bovine parathyroid. *Nature* 366: 575-580, 1993.
7. **Bukoski RD, Bian K, Wang Y, and Mupanomunda M.** Perivascular sensory nerve Ca2+ receptor and Ca2+-induced relaxation of isolated arteries. *Hypertension* 30: 1431-1439, 1997.
8. **Busseuil D, Shi Y, Mecteau M, Brand G, Gillis MA, Thorin E, Asselin C, Romeo P, Leung TK, Latour JG, Des Rosiers C, Bouly M, Rheaume E, and Tardif JC.** Heart rate reduction by ivabradine reduces diastolic dysfunction and cardiac fibrosis. *Cardiology* 117: 234-242, 2010.
9. **Carlson SH, Oparil S, Chen YF, and Wyss JM.** Blood pressure and NaCl-sensitive hypertension are influenced by angiotensin-converting enzyme gene expression in transgenic mice. *Hypertension* 39: 214-218, 2002.
10. **Caroppo R, Gerbino A, Fistetto G, Colella M, Debellis L, Hofer AM, and Curci S.** Extracellular calcium acts as a "third messenger" to regulate enzyme and alkaline secretion. *J Cell Biol* 166: 111-119, 2004.
11. **Cawley T, Geraghty J, Osborne H, and Docherty JR.** Effects of portal hypertension on responsiveness of rat mesenteric artery and aorta. *Br J Pharmacol* 114: 791-796, 1995.
12. **Chang SL, Chen YC, Yeh YH, Lin YK, Wu TJ, Lin CI, Chen SA, and Chen YJ.** Heart failure enhanced pulmonary vein arrhythmogenesis and dysregulated sodium and calcium homeostasis with increased calcium sparks. *J Cardiovasc Electrophysiol* 22: 1378-1386, 2011.
13. **Chang W, Tu C, Chen TH, Bikle D, and Shoback D.** The extracellular calcium-sensing receptor (CaSR) is a critical modulator of skeletal development. *Sci Signal* 1: ra1, 2008.
14. **DeRuiter MC, Gittenberger-De Groot AC, Wenink AC, Poelmann RE, and Mentink MM.** In normal development pulmonary veins are connected to the sinus venosus segment in the left atrium. *The Anatomical record* 243: 84-92, 1995.
15. **Essalihi R, Dao HH, Yamaguchi N, and Moreau P.** A new model of isolated systolic hypertension induced by chronic warfarin and vitamin K1 treatment. *Am J Hypertens* 16: 103-110, 2003.
16. **Feletou M, Huang Y, and Vanhoutte PM.** Endothelium-mediated control of vascular tone: COX-1 and COX-2 products. *Br J Pharmacol* 164: 894-912, 2011.
17. **Fernandez-Rodriguez S, Edwards DH, Newton B, and Griffith TM.** Attenuated store-operated Ca^{2+} entry underpins the dual inhibition of nitric oxide and EDHF-type relaxations by iodinated contrast media. *Cardiovasc Res* 84: 470-478, 2009.
18. **Franklin SS, Gustin Wt, Wong ND, Larson MG, Weber MA, Kannel WB, and Levy D.** Hemodynamic patterns of age-related changes in blood pressure. The Framingham Heart Study. *Circulation* 96: 308-315, 1997.

19. **Garland CJ, Yarova PL, Jimenez-Altayo F, and Dora KA.** Vascular hyperpolarization to beta-adrenoceptor agonists evokes spreading dilatation in rat isolated mesenteric arteries. *Br J Pharmacol* 164: 913-921, 2011.
20. **Guo Q, Huang JA, Yamamura A, Yamamura H, Zimnicka AM, Fernandez R, and Yuan JX.** Inhibition of the Ca(2+)-sensing receptor rescues pulmonary hypertension in rats and mice. *Hypertens Res* 37: 116-124, 2014.
21. **Heiberg E, Sjogren J, Ugander M, Carlsson M, Engblom H, and Arheden H.** Design and validation of Segment--freely available software for cardiovascular image analysis. *BMC Med Imaging* 10: 1, 2010.
22. **Hobaus J, Hummel DM, Thiem U, Fetahu IS, Aggarwal A, Mullauer L, Heller G, Egger G, Mesteri I, Baumgartner-Parzer S, and Kallay E.** Increased copy-number and not DNA hypomethylation causes overexpression of the candidate proto-oncogene CYP24A1 in colorectal cancer. *Int J Cancer* 133: 1380-1388, 2013.
23. **Hofer AM, Curci S, Doble MA, Brown EM, and Soybel DI.** Intercellular communication mediated by the extracellular calcium-sensing receptor. *Nat Cell Biol* 2: 392-398, 2000.
24. **Hofer AM, Gerbino A, Caroppo R, and Curci S.** The extracellular calcium-sensing receptor and cell-cell signaling in epithelia. *Cell calcium* 35: 297-306, 2004.
25. **Holtwick R, Gotthardt M, Skryabin B, Steinmetz M, Potthast R, Zetsche B, Hammer RE, Herz J, and Kuhn M.** Smooth muscle-selective deletion of guanylyl cyclase-A prevents the acute but not chronic effects of ANP on blood pressure. *Proc Natl Acad Sci U S A* 99: 7142-7147, 2002.
26. **Honjo H, Boyett MR, Niwa R, Inada S, Yamamoto M, Mitsui K, Horiuchi T, Shibata N, Kamiya K, and Kodama I.** Pacing-induced spontaneous activity in myocardial sleeves of pulmonary veins after treatment with ryanodine. *Circulation* 107: 1937-1943, 2003.
27. **Kojda G, Laursen JB, Ramasamy S, Kent JD, Kurz S, Burchfield J, Shesely EG, and Harrison DG.** Protein expression, vascular reactivity and soluble guanylate cyclase activity in mice lacking the endothelial cell nitric oxide synthase: contributions of NOS isoforms to blood pressure and heart rate control. *Cardiovasc Res* 42: 206-213, 1999.
28. **Lamprecht MR, Sabatini DM, and Carpenter AE.** CellProfiler: free, versatile software for automated biological image analysis. *Biotechniques* 42: 71-75, 2007.
29. **Lembrechts R, Brouns I, Schnorbusch K, Pintelon I, Kemp PJ, Timmermans JP, Riccardi D, and Adriaensen D.** Functional expression of the multimodal extracellular calcium-sensing receptor in pulmonary neuroendocrine cells. *J Cell Sci* 126: 4490-4501, 2013.
30. **Lepore JJ, Cheng L, Min Lu M, Mericko PA, Morrisey EE, and Parmacek MS.** High-efficiency somatic mutagenesis in smooth muscle cells and cardiac myocytes in SM22alpha-Cre transgenic mice. *Genesis* 41: 179-184, 2005.
31. **Liao R, Podesser BK, and Lim CC.** The continuing evolution of the Langendorff and ejecting murine heart: new advances in cardiac phenotyping. *Am J Physiol Heart Circ Physiol* 303: H156-167, 2012.
32. **Liu L, Wang C, Sun D, Jiang S, Li H, Zhang W, Zhao Y, Xi Y, Shi S, Lu F, Tian Y, Xu C, and Wang L.** Calhex Ameliorates Cardiac Hypertrophy by Inhibiting Cellular Autophagy in Vivo and in Vitro. *Cell Physiol Biochem* 36: 1597-1612, 2015.
33. **Livak KJ and Schmittgen TD.** Analysis of relative gene expression data using real-time quantitative PCR and the 2(-Delta Delta C(T)) Method. *Methods* 25: 402-408, 2001.
34. **Loot AE, Pierson I, Syzonenko T, Elgheznawy A, Randriamboavonjy V, Zivkovic A, Stark H, and Fleming I.** Ca2+ sensing receptor cleavage by calpain partially accounts for altered vascular reactivity in mice fed a high fat diet. *Journal of cardiovascular pharmacology*, 2013.
35. **Marquis RW, Lago AM, Callahan JF, Rahman A, Dong X, Stroup GB, Hoffman S, Gowen M, DelMar EG, Van Wagenen BC, Logan S, Shimizu S, Fox J, Nemeth EF, Roethke T, Smith BR, Ward KW, and Bhatnagar P.** Antagonists of the calcium receptor. 2. Amino alcohol-based parathyroid hormone secretagogues. *J Med Chem* 52: 6599-6605, 2009.
36. **Morimont P, Lambermont B, Desaive T, Janssen N, Chase G, and D'Orio V.** Arterial dP/dtmax accurately reflects left ventricular contractility during shock when adequate vascular filling is achieved. *BMC Cardiovasc Disord* 12: 13, 2012.

37. **Nakagawa K, Parekh N, Koleganova N, Ritz E, Schaefer F, and Schmitt CP.** Acute cardiovascular effects of the calcimimetic R-568 and its enantiomer S-568 in rats. *Pediatr Nephrol* 24: 1385-1389, 2009.
38. **Newaz M, Blanton A, Fidelis P, and Oyekan A.** NAD(P)H oxidase/nitric oxide interactions in peroxisome proliferator activated receptor (PPAR)alpha-mediated cardiovascular effects. *Mutat Res* 579: 163-171, 2005.
39. **Odenwald T, Nakagawa K, Hadtstein C, Roesch F, Gohlke P, Ritz E, Schaefer F, and Schmitt CP.** Acute blood pressure effects and chronic hypotensive action of calcimimetics in uremic rats. *J Am Soc Nephrol* 17: 655-662, 2006.
40. **Ohanian J, Gatfield KM, Ward DT, and Ohanian V.** Evidence for a functional calcium-sensing receptor that modulates myogenic tone in rat subcutaneous small arteries. *Am J Physiol Heart Circ Physiol* 288: H1756-1762, 2005.
41. **Plane F, Wiley KE, Jeremy JY, Cohen RA, and Garland CJ.** Evidence that different mechanisms underlie smooth muscle relaxation to nitric oxide and nitric oxide donors in the rabbit isolated carotid artery. *Br J Pharmacol* 123: 1351-1358, 1998.
42. **Prysyazhna O, Rudyk O, and Eaton P.** Single atom substitution in mouse protein kinase G eliminates oxidant sensing to cause hypertension. *Nat Med* 18: 286-290, 2012.
43. **Riccardi D and Kemp PJ.** The calcium-sensing receptor beyond extracellular calcium homeostasis: conception, development, adult physiology, and disease. *Annu Rev Physiol* 74: 271-297, 2012.
44. **Rietdorf K, Bootman MD, and Sanderson MJ.** Spontaneous, pro-arrhythmic calcium signals disrupt electrical pacing in mouse pulmonary vein sleeve cells. *PloS one* 9: e88649, 2014.
45. **Ruiz A, Lopez RM, Perez T, Castillo C, and Castillo EF.** The effects of NG-nitro-L-arginine methyl ester on systolic pressure, diastolic pressure and pulse pressure according to the initial level of blood pressure. *Fundam Clin Pharmacol* 22: 45-52, 2008.
46. **Rushton DJ, Mattis VB, Svendsen CN, Allen ND, and Kemp PJ.** Stimulation of GABA-induced Ca2+ influx enhances maturation of human induced pluripotent stem cell-derived neurons. *PloS one* 8: e81031, 2013.
47. **Schneider CA, Rasband WS, and Eliceiri KW.** NIH Image to ImageJ: 25 years of image analysis. *Nat Methods* 9: 671-675, 2012.
48. **Schreckenberg R, Dyukova E, Sitdikova G, Abdallah Y, and Schluter KD.** Mechanisms by which calcium receptor stimulation modifies electromechanical coupling in isolated ventricular cardiomyocytes. *Pflugers Arch*, 2014.
49. **Shimokawa H, Yasutake H, Fujii K, Owada MK, Nakaike R, Fukumoto Y, Takayanagi T, Nagao T, Egashira K, Fujishima M, and Takeshita A.** The importance of the hyperpolarizing mechanism increases as the vessel size decreases in endothelium-dependent relaxations in rat mesenteric circulation. *J Cardiovasc Pharmacol* 28: 703-711, 1996.
50. **Smajilovic S, Yano S, Jabbari R, and Tfelt-Hansen J.** The calcium-sensing receptor and calcimimetics in blood pressure modulation. *Br J Pharmacol* 164: 884-893, 2011.
51. **Sward K, Albinsson S, and Rippe C.** Arterial dysfunction but maintained systemic blood pressure in cavin-1-deficient mice. *PloS one* 9: e92428, 2014.
52. **Thakore P and Ho WS.** Vascular actions of calcimimetics: role of Ca(2)(+) -sensing receptors versus Ca(2)(+) influx through L-type Ca(2)(+) channels. *Br J Pharmacol* 162: 749-762, 2011.
53. **Ward DT, Brown EM, and Harris HW.** Disulfide bonds in the extracellular calcium-polyvalent cation-sensing receptor correlate with dimer formation and its response to divalent cations in vitro. *The Journal of biological chemistry* 273: 14476-14483, 1998.
54. **Weston AH, Absi M, Ward DT, Ohanian J, Dodd RH, Dauban P, Petrel C, Ruat M, and Edwards G.** Evidence in favor of a calcium-sensing receptor in arterial endothelial cells: studies with calindol and Calhex 231. *Circ Res* 97: 391-398, 2005.
55. **Yamamura A, Guo Q, Yamamura H, Zimnicka AM, Pohl NM, Smith KA, Fernandez RA, Zeifman A, Makino A, Dong H, and Yuan JX.** Enhanced Ca(2+)-sensing receptor function in idiopathic pulmonary arterial hypertension. *Circ Res* 111: 469-481, 2012.
56. **Yarova PL, Stewart AL, Sathish V, Britt RD, Jr., Thompson MA, AP PL, Freeman M, Aravamudan B, Kita H, Brennan SC, Schepelmann M, Davies T, Yung S, Cholisoh Z, Kidd EJ, Ford WR, Broadley KJ, Rietdorf K, Chang W, Bin Khayat ME, Ward DT, Corrigan CJ, JP**

TW, Kemp PJ, Pabelick CM, Prakash YS, and Riccardi D. Calcium-sensing receptor antagonists abrogate airway hyperresponsiveness and inflammation in allergic asthma. *Sci Transl Med* 7: 284ra260, 2015.
57. **Yu MC, Huang CF, Chang CM, Chen YC, Lin CI, and Chen SA.** Diverse cell morphology and intracellular calcium dynamics in pulmonary vein cardiomyocytes. *Heart Vessels* 26: 101-110, 2011.
58. **Zeidan A, Sward K, Nordstrom I, Ekblad E, Zhang JC, Parmacek MS, and Hellstrand P.** Ablation of SM22alpha decreases contractility and actin contents of mouse vascular smooth muscle. *FEBS Lett* 562: 141-146, 2004.
59. **Ziegelstein RC, Xiong Y, He C, and Hu Q.** Expression of a functional extracellular calcium-sensing receptor in human aortic endothelial cells. *Biochem Biophys Res Commun* 342: 153-163, 2006.
60. **Zitt E, Woess E, Mayer G, and Lhotta K.** Effect of cinacalcet on renal electrolyte handling and systemic arterial blood pressure in kidney transplant patients with persistent hyperparathyroidism. *Transplantation* 92: 883-889, 2011.

Table and figure legends

Table 1. EC_{50} values from wire myography experiments detailed in figures 2 and 3 (see there for experimental conditions) which were fitted with sigmoidal concentration-response curves, with exception of $[Ca^{2+}]_o$ CRC for WT aortas that could not be fitted with the sigmoidal concentration-response curve. Values presented as log(EC_{50}) in mol / L ± SEM. * $p < 0.05$, extra sum-of-squares F-test.

Table 2. Physiological parameters from longitudinal radiotelemetry recordings (*c.f.* Figures 4 and 5) from WT and KO mice kept on control drinking water *vs.* drinking water supplemented with L-NAME (0.5 g / L) and on control diet *vs.* a high salt diet (4 % NaCl-supplemented). Mean ± SEM, N = 5, * / + / # $p < 0.05$, ** / ++ / ## $p < 0.01$, *** / +++ / ### $p < 0.001$, two-way ANOVA with Holm-Sidak post-test, * WT *vs*. KO (post-test); + WT *vs.* KO (ANOVA); # control *vs*. L-NAME / high salt (ANOVA).

Figure 1. Characterization of the $^{SM22\alpha}CaSR^{\Delta flox/\Delta flox}$ mouse. (**A**) Typical genotyping of WT and KO mice. (**B**) Representative histological sections of aortae from WT and KO animals (N=4), scale bars = 100 µm. (**C**) Western blot analysis of CaSR expression with Ponceau staining as loading control (top and middle panel) and α-smooth muscle actin (α-SM actin; bottom panel) expression in endothelium denuded and adventitia-removed, pooled aortae N = 18 (WT), 17 (KO) mice (**D**) Relative mRNA expression of the full-length CaSR (exon 6-7 *vs.* WT) in endothelium-denuded, adventitia-removed aortae of WT and KO animals, mean (line) ± 1SD (box), N = 4, ** $p < 0.01$, Student's t-test (performed on ΔΔCt values *vs.* WT). (**E**) $Ca^{2+}{}_i$ concentration ($[Ca^{2+}]_i$) in freshly isolated WT and KO VSMC exposed to increasing $[Ca^{2+}]_o$ (0.1-5 mmol / L), reported as fold-changes from baseline values. Curves were fitted as

hyperbolic. Mean ± SEM, N = 3 (WT), 4-5 (KO), ** $p < 0.01$, *** $p < 0.001$, two-way ANOVA with Holm-Sidak post-test and, +++ $p < 0.001$, extra sum-of-squares F-test for curve comparison.

Figure 2. Blood vessel contractility of $^{SM22\alpha}CaSR^{\Delta flox/\Delta flox}$ mice is impaired. Aorta (WT, N=33; KO, N=30) and mesenteric artery (MA) responses to (**A**, **B**) high K^+ (KCl, 40 mmol / L; WT, N=33; KO, N=34), (**C**, **D**) phenylephrine (PE, 1 nmol / L – 30 µmol / L), (**E**, **F**) acetylcholine (ACh, 1 nmol / L – 30 µmol / L, PE-preconstricted to ~ 60% max) and (**G**, **H**) Ca^{2+}_o (1-5 mmol / L, PE-preconstricted to ~ 60% max). Results were normalized to the averaged maximum control response in WT. Curves were fitted as sigmoidal concentration-response (for PE and ACh) or third-order polynomial (for Ca^{2+}). Mean ± SEM, * $p < 0.05$, ** $p < 0.01$, *** $p < 0.001$, Student's t-test, or two-way ANOVA with Holm-Sidak post-test, and ++ $p < 0.01$, +++ $p < 0.001$, extra sum-of-squares F-test for curve comparison.

Figure 4. Role of NO in endothelium-dependent relaxation in WT and KO blood vessels. Aorta and mesenteric artery (MA) responses to phenylephrine (PE, 1 nmol / L – 30 µmol / L) (**A**, **B**) in the presence of the NOS inhibitor L-NAME (100 µmol / L) or (**C**, **D**) endothelium denuded (-E). (**E**, **F**) Aorta and MA responses to ACh (1 nmol / L - 30 µmol / L) in the presence of L-NAME (100 µmol / L). (**G**, **H**) Relaxation of endothelium-denuded (-E) aortae and MA from WT and KO mice to increasing concentrations of the NO donor, SNAP. Curves were fitted as sigmoidal concentration-response. Mean ± SEM, * $p < 0.05$, ** $p < 0.01$, *** $p < 0.001$, two-way ANOVA with Holm-Sidak post-test, and +++ $p < 0.001$, extra sum-of-squares F-test for curve comparison.

Figure 3. Pharmacological activation of the CaSR in WT and KO blood vessels. Responses to NPS R-568 (10 nmol / L – 10 µmol / L) in intact (A) or endothelium denuded (B) aortae. Curves were fitted as sigmoidal concentration-response. Mean ± SEM, +++ $p < 0.001$, two-way ANOVA.

Figure 5. Tail cuff and radiotelemetry blood pressure measurements of WT and KO animals. (**A-C**): tail cuff measurements of (**A**) systolic, (**B**) diastolic and (**C**) mean arterial pressures (MAP) of WT and KO mice. Mean ± SEM, N = 20 (WT), 35 (KO), * $p < 0.05$, Student's t-test. (**D-G**): Longitudinal radiotelemetry measurements of (**D**) systolic and (**E**) diastolic blood pressure, (**F**) MAP and (**G**) pulse height (PH) of WT and KO mice in the presence or absence of L-NAME treatment. Mean ± SEM, N = 5 (WT and KO).

Figure 6. Longitudinal radiotelemetry measurements of (**A**) heart rate and (**B**) the positive first derivative of the blood pressure curve (dp/dt) of WT and KO mice in the presence or absence of L-NAME treatment. Mean ± SEM, N = 5 (WT and KO).

Figure 7. Cardiac phenotype of WT and KO animals. (**A**) Haematoxylin and eosin staining and (**B**) Picrosirius red staining (right panels) of heart sections showing reduced occurrence of fibrosis in KO hearts compared to WT. (**C**) Representative long-axis MRI scans and (**D**) 3D reconstructions of left ventricles of WT and remodeled KO mice (5 out of 11 investigated) in end-diastole and end-systole (lower panels). (**E**) Left ventricular mass (LVM), (**F**) left ventricular end diastolic (EDV), (**G**) end systolic (ESV), (**H**) and stroke volume (SV), (**I**) ejection fraction (EF), (**J**) diastolic remodeling index (DRI) and (**K**) wall-thickening (end systolic minus end diastolic wall thickness) of remodeled hearts. N = 5, ** $p < 0.01$, * $p < 0.05$, mean ± SEM, Student's t-test. (**L**) Base intrinsic heart rate (beats per min, bpm) of *ex*

vivo retrograde perfused hearts. N = 9 (WT), 10 (KO), * $p < 0.05$, mean ± SEM, Student's t-test.

Figure 8. Hypothetical mechanism for the CaSR mediated auto-/paracrine amplification of contraction in vascular smooth muscle cells (VSMC). In VSMC, adrenoceptor (AR) agonists (*e.g.* PE) increase Ca^{2+}_i concentration, causing blood vessel constriction. Ca^{2+}_i is then extruded from the cell into the interstitium. Locally accumulating Ca^{2+}_o activates the CaSR on the same and neighboring VSMC, thus amplifying and synchronizing VSMC contractility. Ca^{2+}_i is also extruded into the myo-endothelial space (MES) where it can activate the CaSR on endothelial cell (EC) projections (EP), which penetrate the internal elastic lamina (EL). Activation of the endothelial CaSR leads to VSMC relaxation via a mechanism likely involving NO synthesis and endothelium-derived hyperpolarizations (EDH), in a fashion similar to dilating agents like acetylcholine (ACh) acting on muscarinic receptors (MR).

Legends for supplemental videos

Video S1

Characterization of the cardiac phenotype of $^{SM22\alpha}CaSR^{\Delta flox/\Delta flox}$ mice. Cardiac cine MRI sequence of one heartbeat from three representative WT and three remodeled (5 out of 11 investigated hearts) KO hearts shown in long axis.

Video S2

Characterization of the cardiac phenotype of $^{SM22\alpha}CaSR^{\Delta flox/\Delta flox}$ mice. Representative video of one heartbeat of a WT mouse heart shown as 3D-reconstruction of the left ventricular endocardium (red) intersected with short and long axis image planes (black and white) from cardiac cine MRI.

Video S3

Characterization of the cardiac phenotype of $^{SM22\alpha}CaSR^{\Delta flox/\Delta flox}$ mice. The left ventricle of remodeled hearts from KO mice exhibits full apical closure. Representative video of one heartbeat of a remodeled (5 out of 11 investigated hearts) KO mouse heart shown as 3D-reconstruction of the left ventricular endocardium (red) intersected with short and long axis image planes (black and white) from cardiac cine MRI.

Tables

Table 1

Aorta log(EC_{50}) ± SEM (mol / L)

	Genotype		
Treatment	WT	KO	
PE	-6,871 ± 0,083 (N=19)	-6,534 ± 0,093 (N=18)	*
PE + L-NAME	-7,450 ± 0,106 (N=6)	-7,281 ± 0,145 (N=6)	ns
PE - E	-7,491 ± 0,164 (N=9)	-7,353 ± 0,303 (N=8)	ns
ACh	-7,469 ± 0,095 (N=14)	-7,475 ± 0,067 (N=15)	ns
ACh + L-NAME	-6,150 ± 0,142 (N=4)	-6,146 ± 0,263 (N=5)	ns
SNAP	-6,892 ± 0,167 (N=5)	-6,886 ± 0,279 (N=5)	ns
Calcium	NA	-2,636 ± 0,081 (N=9)	

MA log(EC_{50}) ± SEM (mol / L)

	Genotype		
Treatment	WT	KO	
PE	-5,875 ± 0,080 (N=16)	-5,702 ± 0,070 (N=16)	*
PE + L-NAME	-6,047 ± 0,070 (N=11)	-5,928 ± 0,095 (N=9)	ns
PE - E	-6,352 ± 0,111 (N=10)	-6,263 ± 0,120 (N=11)	ns
ACh	-7.073 ± 0.056 (N=15)	-6.898 ± 0.072 (N=15)	ns
ACh + L-NAME	-6,374 ± 0,161 (N=9)	-6,148 ± 0,182 (N=7)	ns
SNAP	-6,717 ± 0,134 (N=6)	-6,646 ± 0,071 (N=6)	ns
Calcium	-2.832 ± 0,045 (N=10)	-2.782 ± 0,046 (N=9)	ns

Table 2

Night-time	WT	Control	KO		WT	L-NAME	KO			
Systolic (mm Hg)	127.3 ± 4.9	112.1 ± 2.6		*	138.7 ± 5.8	126.7 ± 3.1			++	##
Diastolic (mm Hg)	101.4 ± 4.9	81.3 ± 2.2		**	106.7 ± 4.4	88.9 ± 3.9		**	+++	
MAP (mm Hg)	114.6 ± 4.7	97.3 ± 2.4		*	121.8 ± 4.4	107.1 ± 3.4		*	+++	#
PH (mm Hg)	25.8 ± 2.5	30.8 ± 1.5			32.0 ± 3.4	37.8 ± 1.9			+	#
HR (bpm)	621.1 ± 19.7	515.7 ± 16.1		**	489.3 ± 29.6	409.1 ± 11.4		*	+++	###
dp/dt (mm Hg / s)	1934.9 ± 162.3	2437.2 ± 244.3			1884.5 ± 186.8	2436.9 ± 236.2			+	
Day-time	**WT**	**Control**	**KO**		**WT**	**L-NAME**	**KO**			
Systolic (mm Hg)	108.6 ± 2.3	106.6 ± 2.3			123.9 ± 3.7	118.9 ± 2.5				###
Diastolic (mm Hg)	82.7 ± 1.5	76.8 ± 3.4			95.1 ± 5.6	80.3 ± 3.6		*	+	
MAP (mm Hg)	96.0 ± 1.60	92.01 ± 2.8			109.1 ± 4.1	98.9 ± 3.0			+	##
PH (mm Hg)	26.0 ± 2.0	29.9 ± 1.9			28.8 ± 4.4	38.6 ± 3.0			+	
HR (bpm)	482.8 ± 23.9	459.7 ± 20.0			450.4 ± 23.5	372.2 ± 23.5			+	#
dp/dt (mm Hg / s)	2008.4 ± 95.1	2399.2 ± 259.7			1919.6 ± 279.8	2647.9 ± 261.3			+	

Night-time	WT	Control	KO		WT	High salt	KO			
Systolic (mm Hg)	133.5 ± 1.8	126.6 ± 4.4			133.1 ± 4.5	123.5 ± 3.3			+	
Diastolic (mm Hg)	104.1 ± 1.6	92.4 ± 3.8		**	103.8 ± 1.0	90.5 ± 3.3		**	+++	
MAP (mm Hg)	119.0 ± 1.3	109.7 ± 4.2		*	118.1 ± 2.1	107.1 ± 3.2		*	++	
PH (mm Hg)	29.4 ± 2.0	34.2 ± 1.6			29.3 ± 3.9	33.0 ± 1.1				
HR (bpm)	638.9 ± 2.3	545.3 ± 22.8		**	610.5 ± 19.8	515.2 ± 24.6		**	+++	
dp/dt (mm Hg / s)	2412.1 ± 109.4	2628.5 ± 300.3			2041.8 ± 104.6	2307.4 ± 231.4				
Day-time	**WT**	**Control**	**KO**		**WT**	**High salt**	**KO**			
Systolic (mm Hg)	116.04 ± 3.2	119.4 ± 3.9			114.0 ± 2.6	113.6 ± 1.9				
Diastolic (mm Hg)	87.15 ± 1.6	84.7 ± 4.1			85.6 ± 1.4	78.6 ± 2.3				
MAP (mm Hg)	101.65 ± 2.4	102.0 ± 4.1			99.7 ± 1.5	95.9 ± 1.9				
PH (mm Hg)	28.88 ± 1.8	34.7 ± 2.3			28.5 ± 2.5	35.0 ± 1.9			+	
HR (bpm)	489.0 ± 13.6	457.7 ± 32.8			469.8 ± 14.0	382.9 ± 9.1		*	++	#
dp/dt (mm Hg / s)	2181.7 ± 96.1	2451.4 ± 245.8			2197.5 ± 127.3	2293.6 ± 186.3				

Figures

Figure 1

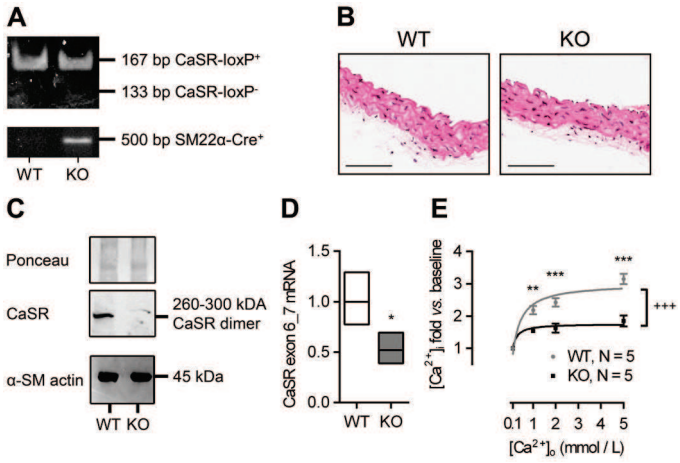

Figure 2

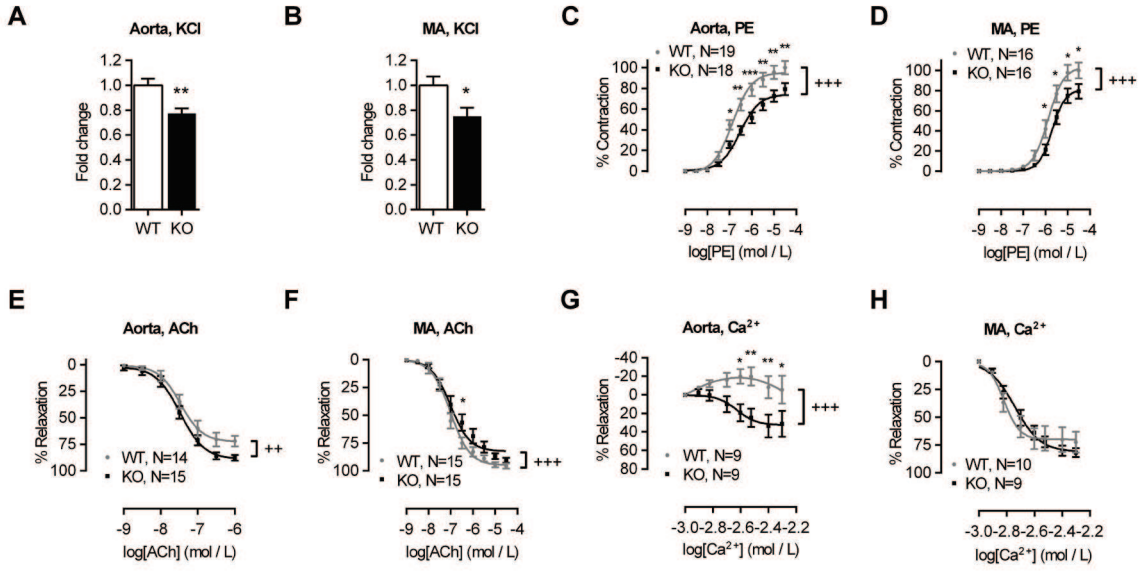
A
Aorta, KCl
Fold change
WT
KO
B
MA, KCl
C
Aorta, PE
WT, N=19
KO, N=18
% Contraction
log[PE] (mol / L)
D
MA, PE
WT, N=16
KO, N=16
E
Aorta, ACh
% Relaxation
WT, N=14
KO, N=15
log[ACh] (mol / L)
F
MA, ACh
WT, N=15
KO, N=15
G
Aorta, Ca2+
WT, N=9
KO, N=9
log[Ca2+] (mol / L)
H
MA, Ca2+
WT, N=10
KO, N=9

Figure 3

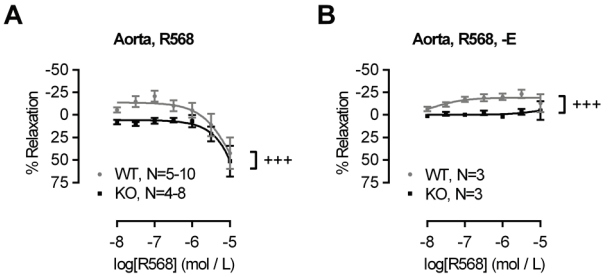
A
Aorta, R568
% Relaxation
-50
-25
0
25
50
75
WT, N=5-10
KO, N=4-8
+++
-8
-7
-6
-5
log[R568] (mol / L)
B
Aorta, R568, -E
% Relaxation
-50
-25
0
25
50
75
WT, N=3
KO, N=3
+++
-8
-7
-6
-5
log[R568] (mol / L)

Figure 4

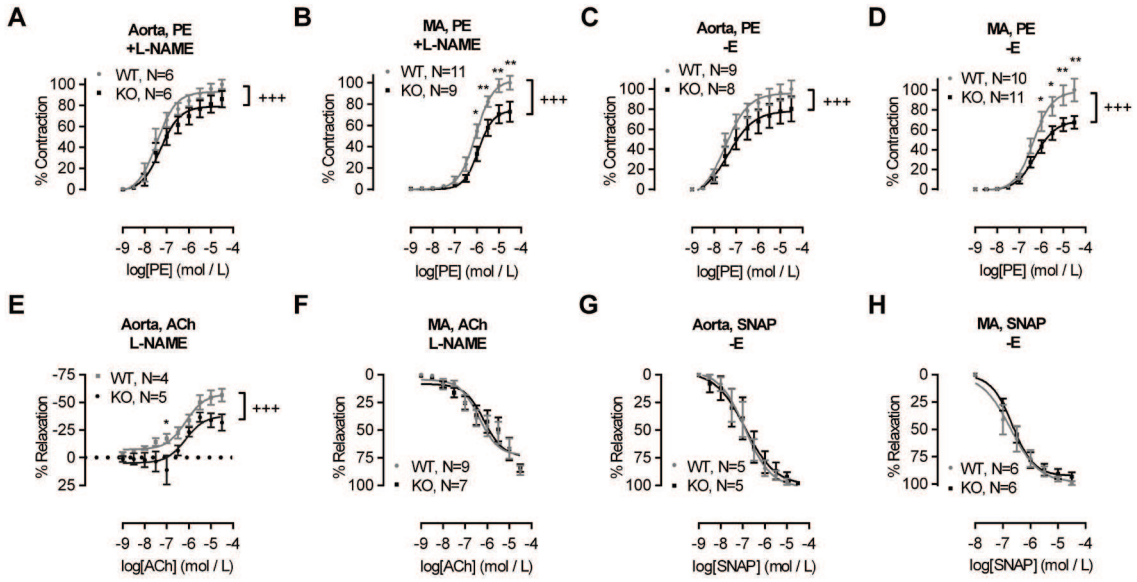
A
Aorta, PE
+L-NAME
WT, N=6
KO, N=6
% Contraction
log[PE] (mol / L)
B
MA, PE
+L-NAME
WT, N=11
KO, N=9
C
Aorta, PE
-E
WT, N=9
KO, N=8
D
MA, PE
-E
WT, N=10
KO, N=11
E
Aorta, ACh
L-NAME
WT, N=4
KO, N=5
% Relaxation
log[ACh] (mol / L)
F
MA, ACh
L-NAME
WT, N=9
KO, N=7
G
Aorta, SNAP
-E
WT, N=5
KO, N=5
log[SNAP] (mol / L)
H
MA, SNAP
-E
WT, N=6
KO, N=6

Figure 5

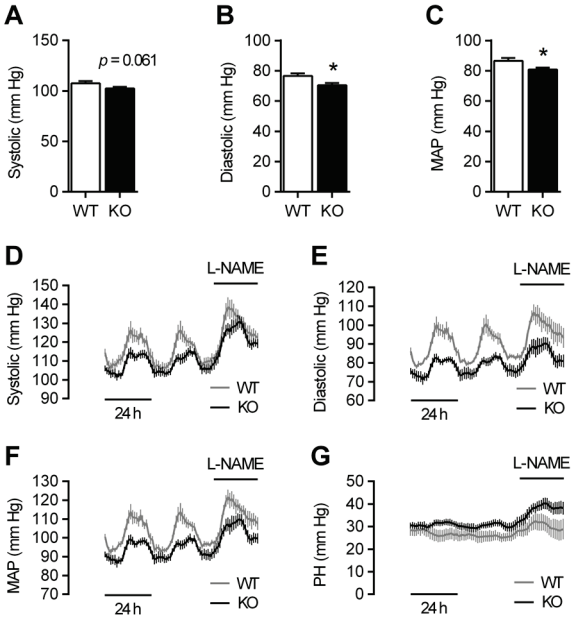
A
B
C
D
E
F
G
Systolic (mm Hg)
Diastolic (mm Hg)
MAP (mm Hg)
PH (mm Hg)
p = 0.061
*
WT
KO
L-NAME
24 h

Figure 6

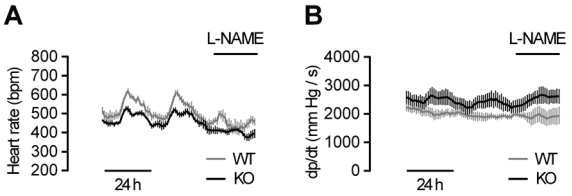
A
L-NAME
Heart rate (bpm)
800
700
600
500
400
300
200
24 h
WT
KO
B
L-NAME
dp/dt (mm Hg / s)
4000
3000
2000
1000
0
24 h
WT
KO

Figure 7

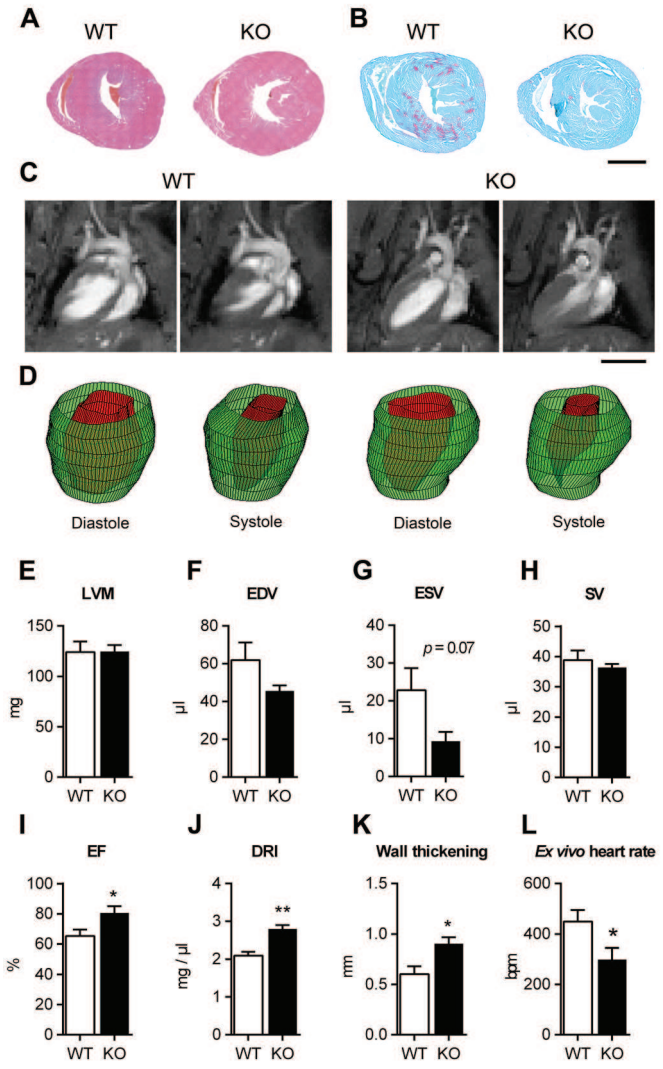
A
WT
KO
B
WT
KO
C
WT
KO
D
Diastole
Systole
Diastole
Systole
E
LVM
mg
F
EDV
µl
G
ESV
p = 0.07
µl
H
SV
µl
I
EF
%
J
DRI
mg / µl
K
Wall thickening
mm
L
Ex vivo heart rate
bpm
WT KO

Figure 8

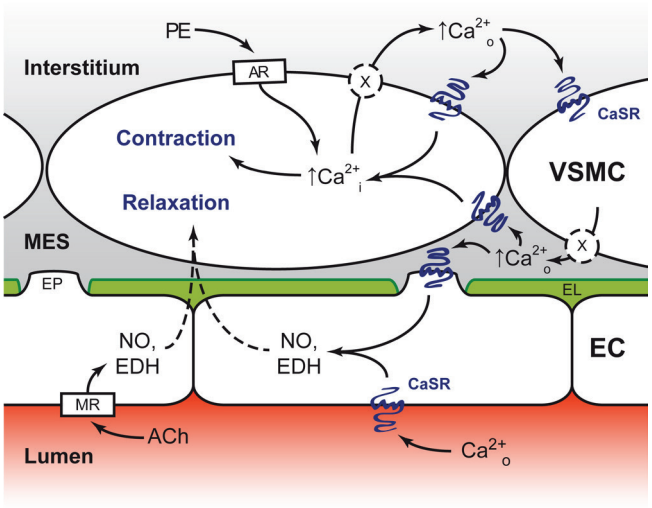
PE
Interstitium
AR
X
↑Ca2+o
CaSR
Contraction
↑Ca2+i
VSMC
Relaxation
MES
↑Ca2+o
X
EP
EL
NO,
EDH
NO,
EDH
EC
CaSR
MR
ACh
Lumen
Ca2+o